Materials Today Bio 22 (2023) 100739

Contents lists available at ScienceDirect

Materials Today Bio

journal homepage: www.journals.elsevier.com/materials-today-bio

Zn^{2+} incorporated composite polysaccharide microspheres for sustained growth factor release and wound healing

Yikun Ju [a,b], Huanxuan Zeng [a], Xiuzhi Ye [a], Minghai Dai [a], Bairong Fang [b,**], Liangle Liu [a,*]

[a] The Third Affiliated Hospital of Wenzhou Medical University, Wenzhou, 325200, China
[b] Department of Plastic and Aesthetic (Burn) Surgery, The Second Xiangya Hospital, Central South University, Changsha, 410011, China

ARTICLE INFO

Keywords:
Microspheres
Zinc
Polysaccharide
Wound healing
Double cross-linked

ABSTRACT

The development of new wound dressings has always been an issue of great clinical importance and research promise. In this study, we designed a novel double cross-linked polysaccharide hydrogel microspheres based on alginate (ALG) and hyaluronic acid methacrylate (HAMA) from gas-assisted microfluidics for wound healing. The microspheres from gas-assisted microfluidics showed an uniform size and good microsphere morphology. Moreover, this composite polysaccharide hydrogel microspheres were constructed by harnessing the fact that zinc ions (Zn^{2+}) can cross-link with ALG as well as histidine-tagged vascular endothelial growth (His-VEGF) to achieve long-term His-VEGF release, thus promoting angiogenesis and wound healing. Meanwhile, Zn^{2+}, as an important trace element, can exert antibacterial and anti-inflammatory effects, reshaping the trauma microenvironment. In addition, photo cross-linked HAMA was introduced into the microspheres to further improve its mechanical properties and drug release ability. In summary, this novel Zn^{2+} composite polysaccharide hydrogel microspheres loaded with His-VEGF based on a dual cross-linked strategy exhibited synergistic antimicrobial and angiogenic effects in promoting wound healing.

1. Introduction

The skin serves as a vital barrier for the human body, protecting it from damage caused by exogenous harmful substances [1,2]. When the epidermis undergoes damage due to trauma or other factors, the wounds get directly exposed to the outside air and risk bacterial infection, which leads to prolonged healing times [3–6]. Chronic non-healing wounds present a significant clinical challenge. They impose a major burden on both patients and society [3–5]. Controlling or preventing wound infections can effectively promote efficient healing [7]. However, through the misuse of antibiotics, bacteria have gradually developed antibiotic resistance [7,8]. Therefore, further development in antimicrobial-based dressings has high clinical and economic benefits [3–5]. Recently, a wide range of biomaterials has been extensively studied regarding the treatment of various traumas, with many showing great potential [6,7,9].

Hydrogels are a common biomaterial with a three-dimensional network structure. They are considered excellent materials for wound dressing because of their good drug-carrying capacity, water absorption, and moisture retention [10,11]. Currently, there is considerable focus on hydrogels based on natural materials with good biocompatibility, degradability, and similarity to the natural extracellular matrix (ECM) [9]. Conventional block hydrogels have certain application limitations, especially when requiring injections or smaller sizes. Hydrogel microspheres are a class of micro-sized hydrogel particles (~1–1000 μm) and demonstrate more adaptability in the biomedical field than bulk hydrogels because they can be injected through syringes or catheters, facilitating minimally invasive delivery of biological agents [12]. Microfluidics refers to a system(s) that uses microtubules (tens to hundreds of microns in size) to handle or manipulate tiny fluids, and is now commonly used in the preparation of hydrogel microspheres [13,14]. Hydrogel microspheres prepared by gas-assisted microfluidics are uniform in size and have good micromorphological characteristics [15–17]. Alginate (ALG) is a marine polysaccharide with good biocompatibility. It can cross-link with divalent cations and form hydrogels by physical cross-linking [18]. Hyaluronic acid is also a common natural polysaccharide and is one of the main components of the ECM [19]. By modification of hyaluronic acid through methacrylation, a hyaluronic acid methacrylate (HAMA) with photo-cross-linking properties can be obtained, which is extensively used in biomedical applications [20].

* Corresponding author.
** Corresponding author.
E-mail addresses: fbrfbr2004@csu.edu.cn (B. Fang), liuliangle@wmu.edu.cn (L. Liu).

https://doi.org/10.1016/j.mtbio.2023.100739
Received 8 April 2023; Received in revised form 17 June 2023; Accepted 19 July 2023
Available online 20 July 2023

Zinc ions (Zn^{2+}) is a crucial trace element in the human body and is widely involved in the synthesis of various living substances [21,22]. It plays an important role in several trauma-healing processes, including cell proliferation, cellular immune regulation, and ECM deposition [21]. Prolonged Zn^{2+} deficiency in humans can lead to retarded growth and poor healing of skin wounds. Some studies have shown that certain chronic wounds are accompanied by a loss of Zn^{2+} [23]. In addition, Zn^{2+} demonstrates antibacterial activity [24]. Sukhodub et al. [25] evaluated chitosan alginate hydrogel dressings based on different metal ions and found that the Zn^{2+} based hydrogels showed excellent broad-spectrum antimicrobial properties. Therefore, Zn^{2+} are expected to be a critical component of new trauma dressings. Recently, researchers have constructed a hydrogel dressing compounded with Zn^{2+} and magnesium ions, showing that Zn^{2+} promotes fibroblast migration and contributes to wound healing [22,26].

Vascular endothelial growth factor (VEGF) is a prominent class of pro-angiogenic factors that promote migration, proliferation, and angiogenesis of vascular endothelial cells. Numerous studies have shown that VEGF can promote wound healing by promoting trabecular angiogenesis [27,28]. However, the direct application of VEGF occurs with transient clearance, making it difficult to exert a sustained effect [28]. Since wound healing is a long-term process, sustained low doses of VEGF can be more effective than administering a single high dosage, especially for chronic refractory wounds [28]. However, loading VEGF by purely physical adsorption leads to a skewed release of VEGF [29]. Since His-tag can bind to divalent metal ions, we use His-tagged VEGF (His-VEGF) to achieve a slow release via physical and chemical cross-linking [30].

In this study, we propose the construction of Zn^{2+}-based His-VEGF-loaded double cross-linked hydrogel microspheres for treating infected wounds (Fig. 1). The ALG is a linear polymer with three chain segments connected by glycosidic bonds and two secondary hydroxyl groups in each structural unit of the molecule, all of which have the reactive properties of alcoholic hydroxyl groups. The sodium ion (Na^{+}) on the ALG unit can undergo an ion-exchange reaction with Zn^{2+}, enabling the coordination of the carboxyl group of ALG with Zn^{2+}. The ALG units can stack to form a cross-linked network structure, forming a hydrogel. HAMA was also added to give the hydrogel microspheres photo-cross-linking properties. We prepared double cross-linked hydrogel microspheres (MS) based on metal ion coordination and ultraviolet (UV) cross-linking using nitrogen (N_2)-assisted microfluidic technology. As the histidine tag (His-tag) can also be ligated with Zn^{2+}, we loaded His-VEGF into MS and constructed MS@His-VEGF, which can slowly release VEGF. The double cross-linking property prolongs the time of VEGF release, with Zn^{2+} also released upon degradation of the microspheres, which can exert certain anti-inflammatory and antibacterial effects. In conclusion, the MS@His-VEGF designed in this study can achieve anti-inflammatory and antibacterial properties along with slowly releasing VEGF, giving it good application prospects for chronic wound management.

2. Results and discussion

2.1. Characterization of MS@His-VEGF

As mentioned above, Zn^{2+} can cross-link with both ALG and His-VEGF. HAMA was also introduced to further cross-link the microspheres by UV light. Double cross-linking enhances the stability of the microspheres while enabling the slow release of VEGF. MS@His-VEGF prepared by N_2-assisted microfluidics appears milky white and

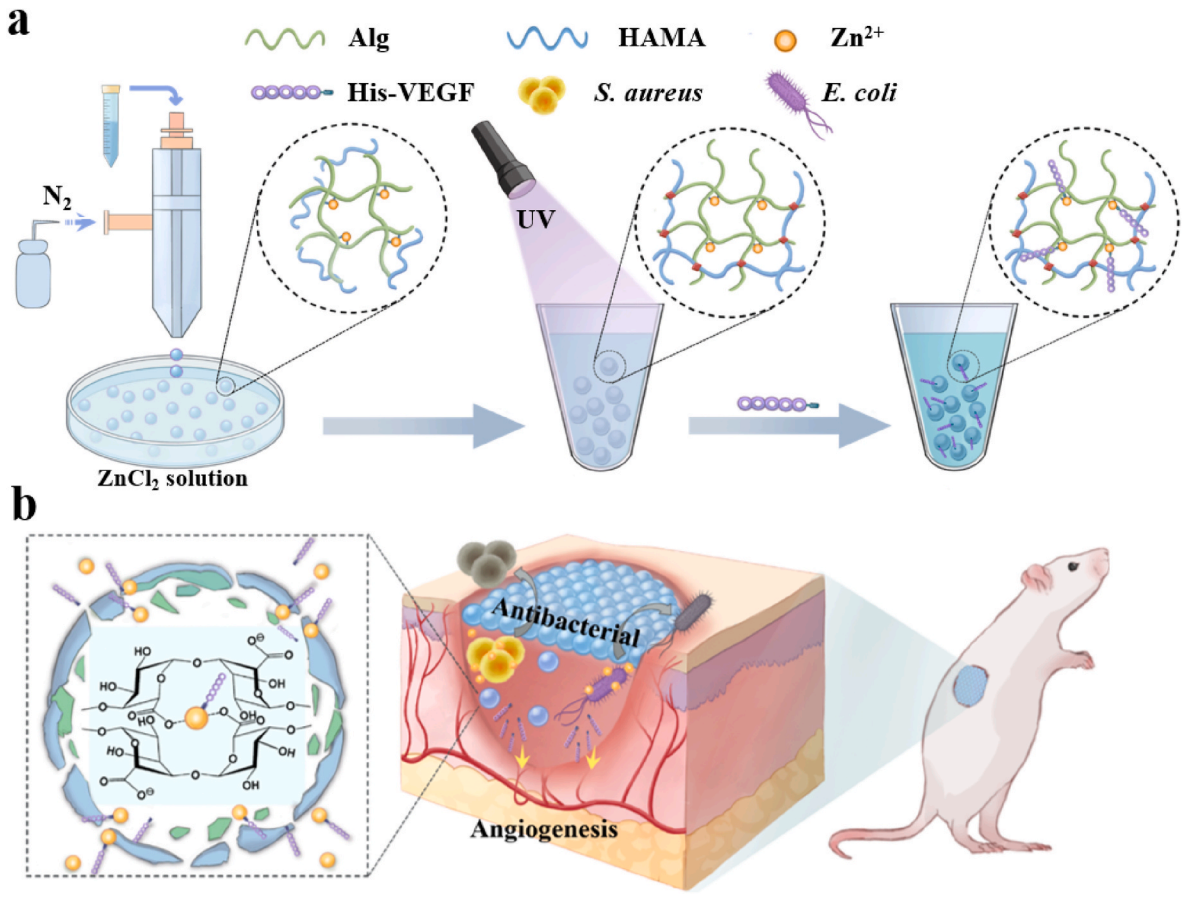

Fig. 1. Zn^{2+} incorporated composite polysaccharide microspheres for sustained growth factor release and wound healing. (a) Schematic diagram of the preparation of hydrogel microspheres. (b) Schematic diagram of the release of His-VEGF from microsphere for wound healing.

translucent in its microparticle form to the naked eye (Fig. 2 a). It was analyzed using a light microscope, and a uniform spherical shape with a smooth surface was observed, with a particle size distribution of around 230 μm (Fig. 2 b, c). The microscopic morphology of the microspheres was analyzed by scanning electron microscopy, and the microspheres prepared by double cross-linking showed dense and stable spherical shapes (Fig. 2 d, e, f). The composition of the microspheres was evaluated via elemental analysis. Zn^{2+} was verified as the main component constituting MS@His-VEGF and, therefore, plays an important role (Fig. 2 g, h, i). We evaluated the effect of the cross-linking mode on the degradation rate of hydrogel microspheres. MS that did not undergo HAMA photo-crosslinking were almost completely degraded within 3 days at 37 °C. In contrast, MS that underwent double cross-linking still had a retention rate of 37.45% at day 7 (Figure S1).

2.2. *In vitro drug release and antibacterial properties*

Controlling the efficiency of drug release can prevent transient drug clearance and achieve better therapeutic results. Previous studies have shown that His-tags can chelate divalent metal ions, prolonging the release of His-tagged drugs [30]. The *in vitro* drug release profile results show that His-VEGF could be loaded more efficiently into the microspheres. The release time of the drug was prolonged, with the release of His-VEGF observable over a period of up to 7 d. Smaller doses of drugs, enabled by slow-release mechanisms, benefit the healing process of the wound and can provide better therapeutic results [1,31]. Moreover, we analyzed the effect of the cross-linking method on the loaded drug. The release time of both VEGF and His-VEGF was prolonged after performing photo-crosslinking. A possible reason for this is the double cross-linking method enhanced the cross-linking strength and the stabilization of the hydrogel microspheres (Figure S2). Additionally, with the degradation and absorption of MS@His-VEGF, trace amounts of Zn^{2+} are also released into the wound, which can influence antibacterial and synergistic tissue repair. We evaluated the release of Zn^{2+} from MS@His-VEGF using inductively coupled plasma emission spectroscopy (ICP-AES). The release profile of Zn^{2+} showed a continuous release. Approximately 1.87 ppm of Zn^{2+} was released from the MS@His-VEGF within 7 d (Figure S3).

Staphylococcus aureus (*S.aureus*) and *Escherichia coli* (*E.coli*) are classic examples of bacteria. They are representative of gram-positive and gram-negative bacteria. Previous studies have reported Zn^{2+} possessing broad-spectrum antibacterial effects [26]; hence, the prepared MS and MS@His-VEGF were tested for its antibacterial properties. The bacterial count significantly reduced post co-culturing using MS and MS@His-VEGF with the above-cited bacteria. The results of the bacterial coating experiments revealed a considerable reduction in the bacterial colonies after treatment (Fig. 3 a, b). The number of live and dead bacteria was evaluated by the Live & Dead Bacterial Staining Kit, with the results showing a sizeable increase in the percentage of dead bacteria after treatment (Fig. 3 c, d). After the treated bacteria are collected, fixed, dehydrated, and after surface gold spraying, their microscopic morphology is observed under SEM. Compared to the control group, both MS and MS@His-VEGF caused the bacteria to shrink and rupture, leaving them out of their normal morphology (Fig. 3 e). The prepared MS@His-VEGF exhibited broad-spectrum antibacterial properties; the addition of His-VEGF did not affect the antibacterial performance of MS.

2.3. *Biocompatibility*

To evaluate the biocompatibility of the prepared microspheres, the

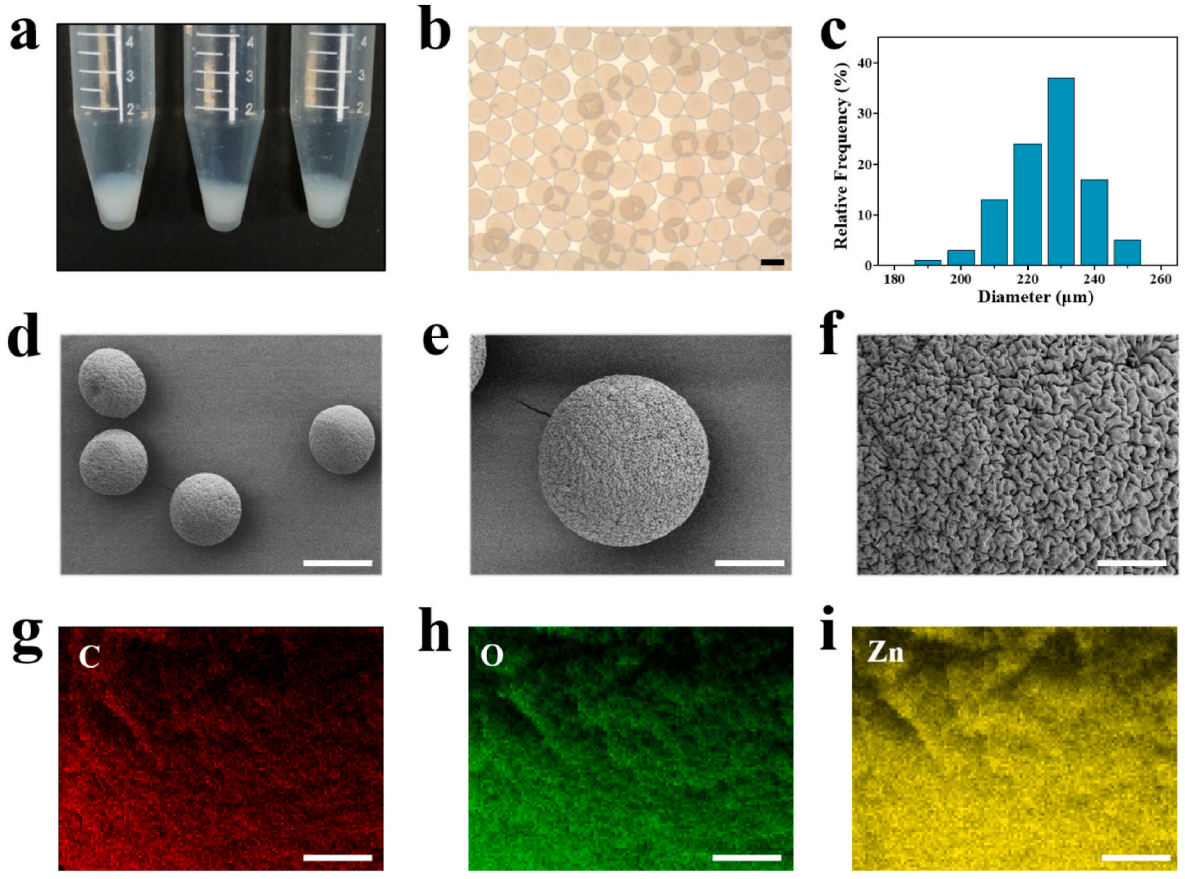

Fig. 2. Characterization of MS@His-VEGF. (a) General shape. (b) Morphology under optical microscope. (c) Particle size distribution. (d–i) SEM images and elemental analysis of MS@His-VEGF. The scale bars are 200 μm, 150 μm, 50 μm in (b), (d), (e), and 20 μm in (f), (g), (h), (i) respectively.

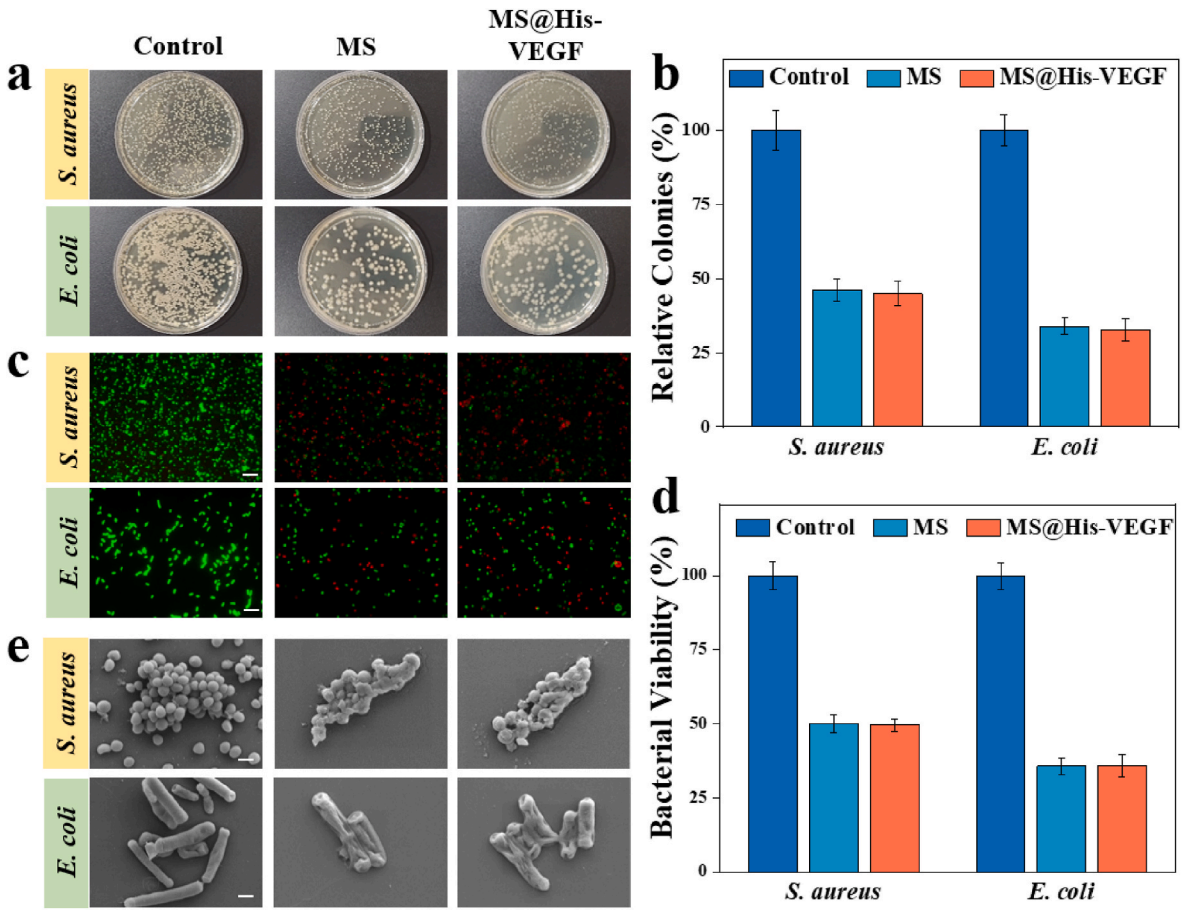

Fig. 3. Antibacterial properties of MS@His-VEGF. (a) The antibacterial ability of MS and MS@His-VEGF against *S. aureus* and *E. coli* were detected by spread plate method. (b) Statistical graph of the number of colonies. (c) Fluorescence photograph of live-dead staining of *S. aureus* and *E. coli.* (d) Statistical analysis of living/dead bacteria. (e) SEM images of *S. aureus*. and *E. coli*. The scale bars are 10 μm in (c), 2 μm in (e), respectively.

cytotoxicity of the microspheres was determined using the cell live/dead staining method as well as the Cell Counting Kit 8 (CCK8) method. Human umbilical vein endothelial cells (HUVEC) and human skin fibroblast cells (HSF) were used to evaluate the effect of the microspheres on cytotoxicity (Fig. 4 a). The results showed that on day 3, HUVEC in the MS@His-VEGF group experienced a significant increase in the proliferated cells than the control group (Fig. 4 b, Figure S4). There was no difference in the survival rate of HSF groups on day 3 (Fig. 4 c). The prepared microspheres did not appear to be cytotoxic. We evaluated the hematotoxicity of MS and MS@His-VEGF via hemolysis assay. The results showed that the prepared microspheres had good hemocompatibility (Figure S5). In addition, we obtained the heart, liver, spleen, lungs, kidneys and subcutaneous tissue. We implanted MS@His-VEGF subcutaneously and executed them after 7 d to assess potential organ toxicity. The results showed no noticeable abnormal alterations in organ pathological staining compared to normal mice (Figure S6).

2.4. *In vitro pro-angiogenesis*

VEGF, an important vasoactive substance, promotes the proliferation, migration and tube-forming ability of HUVEC. The pro-angiogenic capacity of MS@His-VEGF was evaluated to demonstrate the biological activity of the released His-VEGF. The results of the cell scratch assay showed that the MS@His-VEGF group had significantly better cell migration ability than the control and MS groups at 24 h (Fig. 5 a, c). In addition, the results of the tube formation assay indicated that the MS@His-VEGF group displayed stronger tube formation ability at 6 h (Fig. 5 b, d). In summary, His-VEGF released by MS@His-VEGF is biologically active and can significantly promote angiogenesis.

2.5. *Promote the healing of infected wounds*

To further confirm that MS@His-VEGF promotes infected wound healing *in vivo*, mice with were randomly divided into different groups and infected wound models were created. Mice were treated with different treatments and the healing process was recorded for 8 d (Fig. 6 a). The results showed that MS@His-VEGF could promote wound healing more significantly when compared to MS or His-VEGF-only treatment (Fig. 6 c). Since MS@His-VEGF has a good antibacterial effect, it can provide a suitable microenvironment for the healing of wounds. It can also exert anti-inflammatory and pro-angiogenic effects through the sustained release of Zn^{2+} and His-VEGF. MS@His-VEGF can act synergistically to promote the healing of infected wounds. The mice were euthanized on day 9, and the skin tissue around the wound was fixed and stained. The histological changes of the wounds were evaluated by using hematoxylin-eosin (H&E) staining (Fig. 6 b). The H&E results showed that the wounds in the MS@His-VEGF group healed more completely at the base and were significantly thicker than the other groups (Fig. 6 d). We also evaluated the effect of the MS@VEGF and MS@His-VEGF groups on wound healing separately. Both significantly promoted wound healing, with the MS@His-VEGF group being relatively a little more effective (Figure S7). We speculate that the possible reason is the sustained release of VEGF at very low doses, which is more consistent with the biological process of wound healing [1,31]. Particularly in chronic wounds, where MS@His-VEGF may show better efficacy.

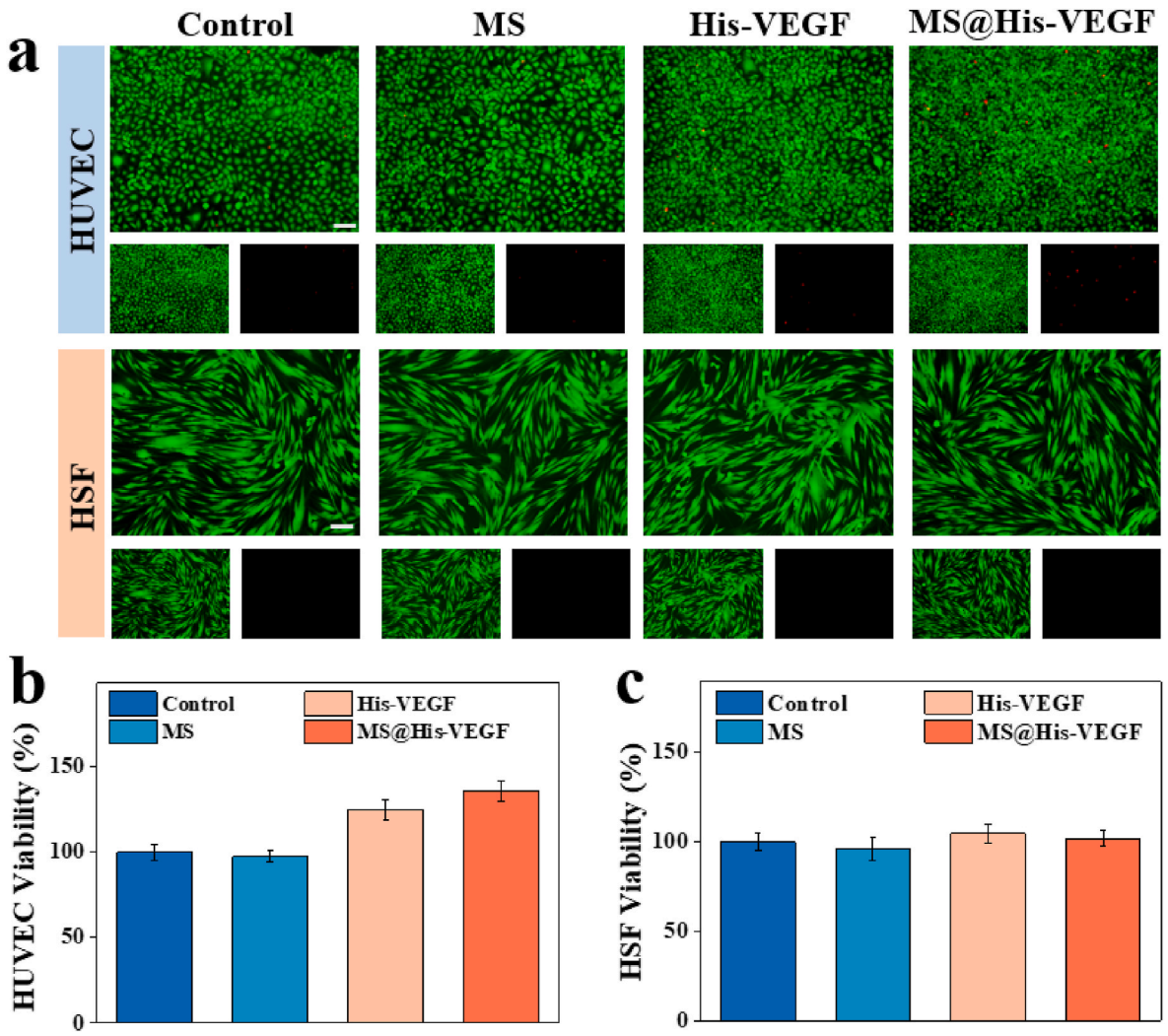

Fig. 4. Biocompatibility of MS@His-VEGF. (a) Live/dead fluorescent images (green: live cells, red: dead cells) of HUVEC cells and HSF cells after culturing with different groups for 3 days. (b), (c) CCK-8 assays. The scale bar is 100 μm. (For interpretation of the references to color in this figure legend, the reader is referred to the Web version of this article.)

2.6. Analysis of collagen deposition and proinflammatory factors

To evaluate the healing of the wounds tissue at the pathological level, the collagen deposition in the skin tissue was evaluated by using Masson staining. Collagen deposition was most pronounced in the His-VEGF group and the MS@His-VEGF group than the control group. The MS group also had more collagen deposition compared to the control group, but was weaker than the His-VEGF and MS@His-VEGF groups (Fig. 7 a, b). The expression of the inflammatory index interleukin (IL-6) as well as tumor necrosis factor Alpha (TNF-α) was evaluated by using immunohistochemical staining. IL-6 is involved in host defense against pathogens in the environment, and IL-6 levels respond to the inflammatory response generated locally by the tissues [32]. A drop in IL-6 levels occurs when the stressor (e.g., bacteria) is removed from the host. Conversely, persistent high IL-6 levels lead to a prolonged inflammatory response, which affects wound healing and is associated with the development of chronic refractory wounds. Immunohistochemical staining results showed that IL-6 expression levels were significantly decreased in the MS group versus the MS@His-VEGF group compared to the control group (Fig. 7 a, c). The release of Zn^{2+} has antibacterial and anti-inflammatory effects and reduces the inflammatory response of the wounds tissue. TNF-α is a small molecule protein secreted by macrophages and is a common indicator of inflammation [33]. TNF-α is a pro-inflammatory factor that promotes the proliferation and differentiation of immune cells and plays an important role in the body's immune activity. However, excessive TNF-α can damage vascular endothelial cells and influence angiogenesis [33]. The results of immunohistochemistry showed that TNF-α expression decreased in all the remaining groups compared to the control group (Fig. 7 a, d). The reduced inflammatory factors in the His-VEGF group could be due to angiogenesis. Angiogenesis is important in wound healing. The formation of new capillaries near the wound surface increases blood perfusion to the wound surface, providing the surrounding tissue cells with the nutrients necessary for growth, while removing cellular metabolites [34]. The above results show that our prepared MS@His-VEGF has a positive anti-inflammatory effect and can effectively alleviate the inflammatory response of the wound tissue.

2.7. Neovascularization

To assess the role of MS@His-VEGF in promoting angiogenesis in animals *in vivo*, we used cluster of differentiation 31 (CD31) and α-smooth muscle actin (α-SMA) immunofluorescence staining to assess the level of angiogenesis. CD31 and α-SMA are common markers for the evaluation of neovascularization. The results of immunofluorescence showed a significant increase in the density and degree of

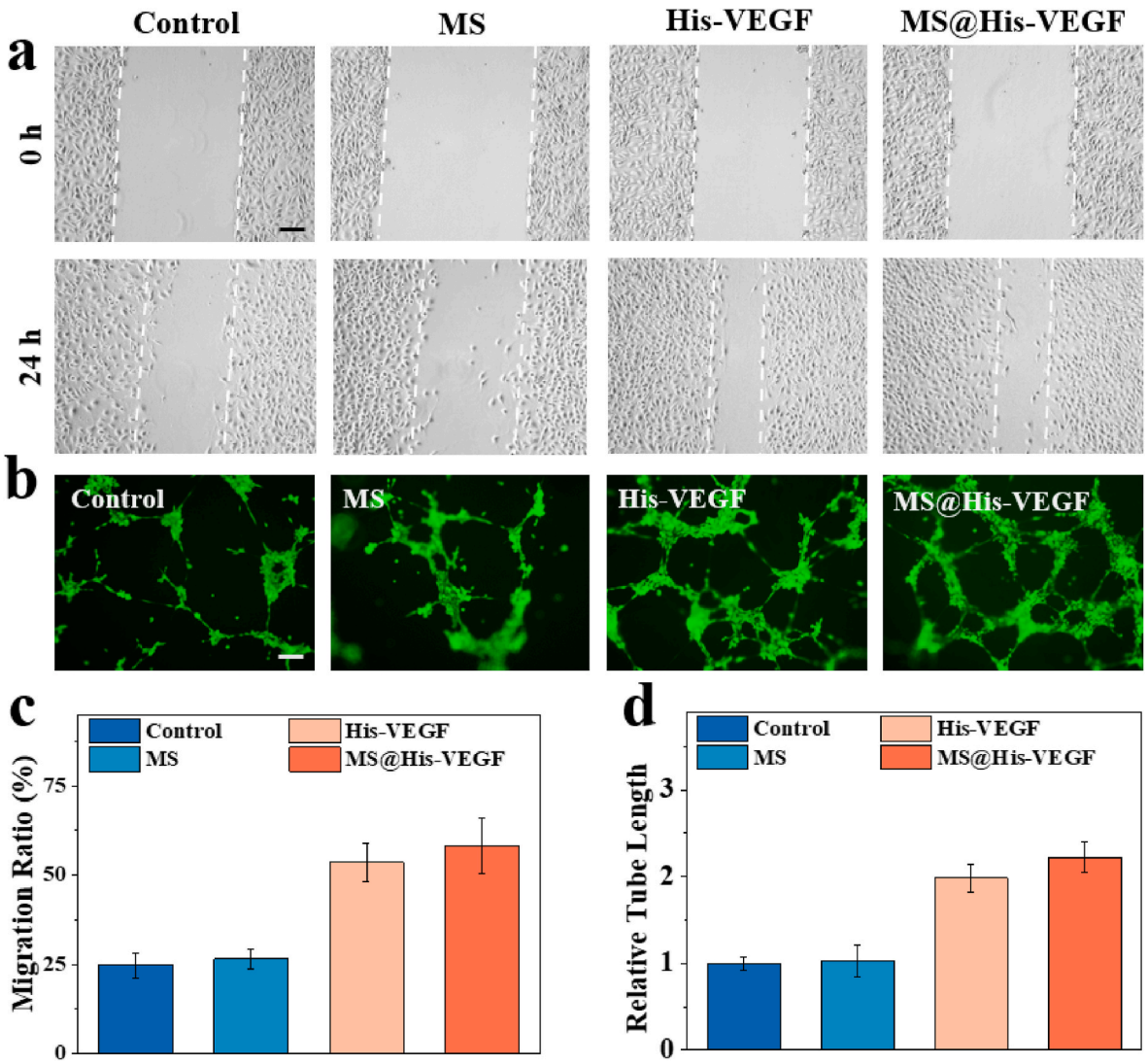

Fig. 5. Scratch and tube formation experiments. (a) HUVEC migration in different treatments. (b) HUVEC tube formation in different treatments. (c) Quantitative analysis of cell migration rate. (d) Quantitative analysis of the length of tube formation. The scale bar is 100 μm.

neovascularization in the MS@His-VEGF group compared to the other groups (Fig. 8). It indicates that the prepared MS@His-VEGF can effectively load His-VEGF, while the released His-VEGF has the effect of promoting angiogenesis *in vivo*, in agreement with the conclusions of previous cellular experiments.

3. Conclusion

In conclusion, we prepared a novel composite polysaccharide microsphere based on a property of Zn^{2+} that it can cross-link with ALG and His-VEGF, and further photo-cross-linked it using HAMA. The prepared composite polysaccharide hydrogel microspheres displayed good stability and biocompatibility. Due to the double cross-linking property, His-VEGF is tightly bound to the hydrogel microspheres, achieving a long-term slow release of His-VEGF. The slow-release properties are better matched to the physiological cycle of wound healing, thus allowing for better efficacy. At the same time, Zn^{2+} plays an important role in wound healing. As an important trace element, Zn^{2+} can play antibacterial and anti-inflammatory roles, providing a favorable microenvironment for wound healing. The above features suggest that Zn^{2+}-based double cross-linked hydrogel microspheres can achieve efficient loading of His-VEGF as well as long-lasting release, while exerting antibacterial and anti-inflammatory influence to synergistically promote wound healing.

4. Materials and methods

4.1. Materials

ALG and $ZnCl_2$ were purchased from Sigma (St. Louis, USA). HAMA was acquired from Engineering for Life (Suzhou, China). VEGF and His-VEGF were purchased from Abcam (Shanghai, China). Matrigel was purchased from BD Bioscience (Shanghai, China). Calcein-AM/PI and Cell Counting Kit-8 were purchased from Applygen (Beijing, China). Live & Dead Bacterial Staining Kit was purchased from Yeason (Shanghai, China). VEGF ELISA kits were purchased from Multi Sciences (Hangzhou, China). HSF and HUVEC were obtained from Muke Biotech (Wenzhou, China). DMEM, Fetal Bovine Serum (FBS) and phosphate buffered saline (PBS) were obtained from Gibco, Thermo Fisher Scientific (Suzhou, China). Masson's trichrome staining and H&E staining kits were obtained from Servicebio (Wuhan, China). All antibodies were purchased from Abcam (Cambridge, UK). Eight-week-old C57/BL6J mice were purchased from Jiake Biotechnology (Shanghai, China). All animal study protocols were approved by the Institutional Animal Care and Use Committee of Wenzhou Medical University(wydw2023-0142).

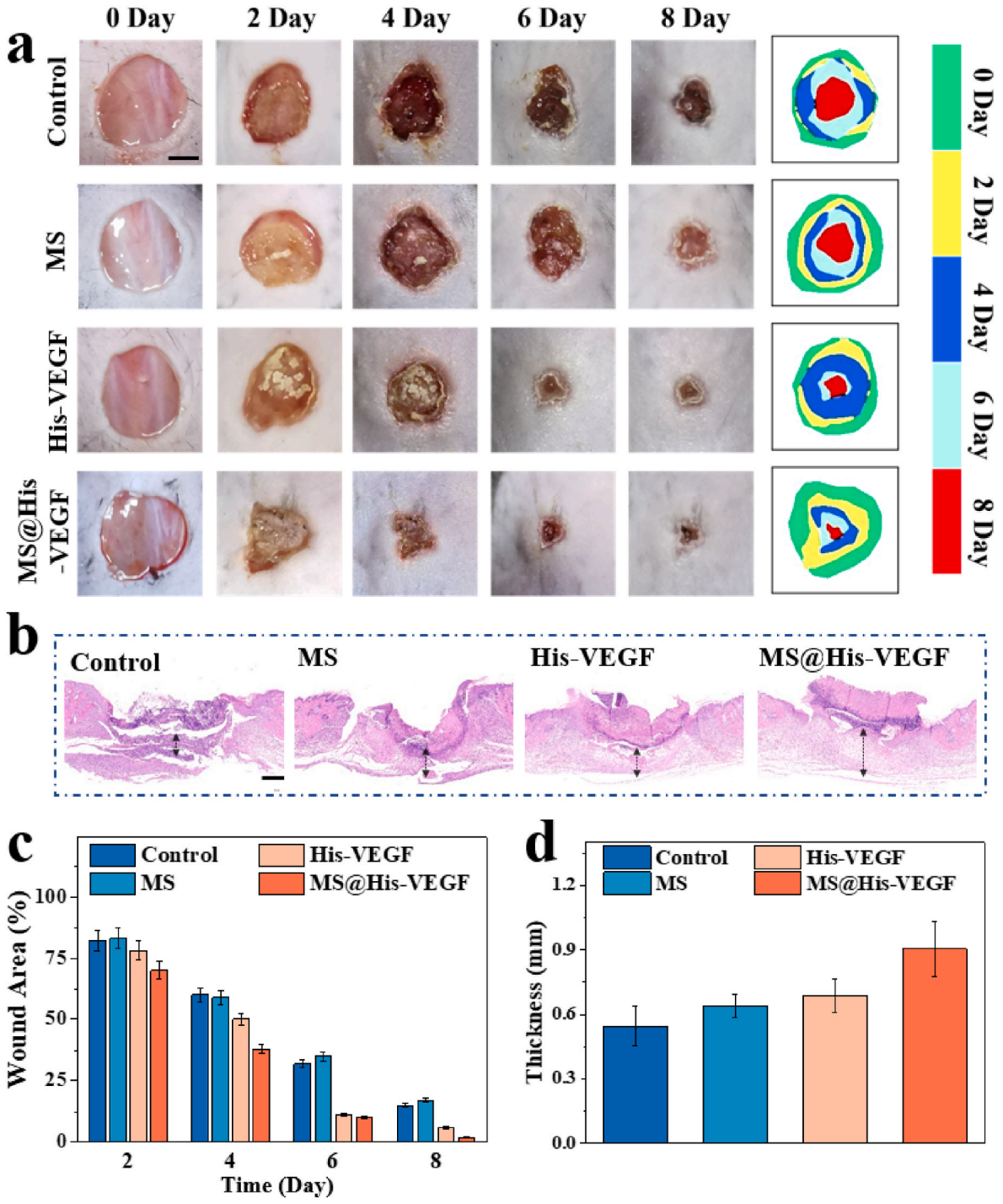

Fig. 6. Wound healing and histological analysis. (a) Photos of the wounds in the different treatment groups at day 0,2,4,6,8. (b) H&E staining in different groups. (c) Quantification analysis of wound closure at day 2, 4, 6 and 8. (d) Quantitative analysis of the basal thickness of the wound. The scale bars are 5 mm in (a) and 500 μm in (b).

4.2. Preparation of MS@His-VEGF

We prepared a double cross-linked hydrogel microspheres by N_2 blow-off method combined with UV light curing. The solution containing 2 %ALG and 5%HAMA was squeezed out drop by drop through the microfluidic devices with the assistance of N_2 purge, so that the large droplets were broken up into small uniform droplets. Small droplets fell into the container containing $ZnCl_2$ solution below, and Zn^{2+} cross-linked with ALG and polymerized into hydrogel microspheres. Here, the crosslinking was rapid and small droplets crosslinked to form microspheres within 30 s after being added into the $ZnCl_2$ solution. Next, they were further cross-linked using UV irradiation for 30 min. The resulting microspheres were collected into centrifuge tubes and washed repeatedly using ultrapure water to remove any uncross-linked Zn^{2+}. The cleaned microspheres were transferred to a PBSsolution containing His-VEGF and then incubated at room temperature for 1 h. His-tag can be cross-linked with Zn^{2+}, thus allowing His-VEGF to be loaded into the microspheres. The microspheres prepared by double cross-linking have good stability and maintain a stable morphology in pure aqueous solutions as well as in PBS solutions. In addition, the microscopic

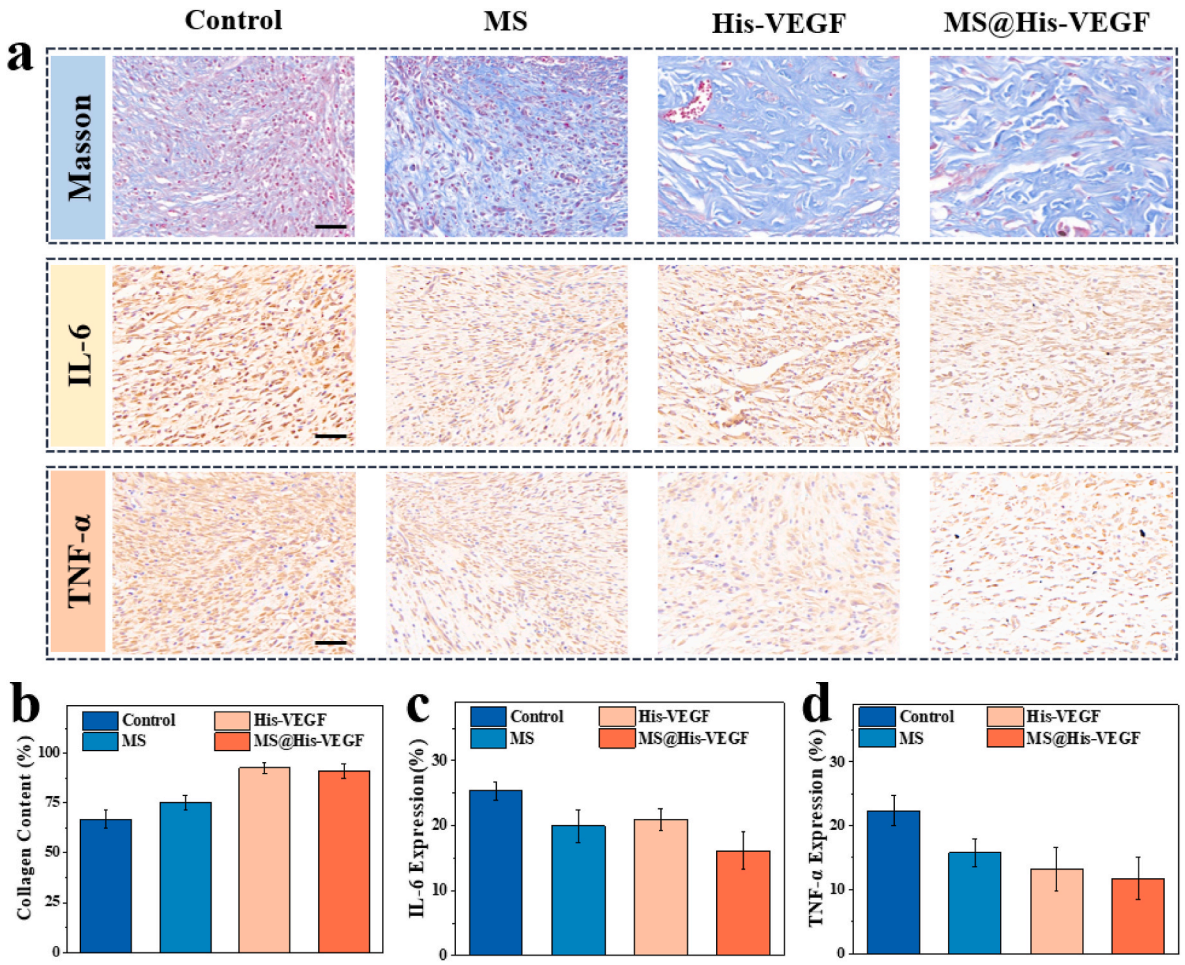

Fig. 7. Analysis of collagen deposition and proinflammatory factors. (a) Staining of collagen, IL-6, and TNF-α. (b–d) Quantitative analysis of collagen deposition, IL6, and TNF-α in different groups. The scale bars are 50 μm.

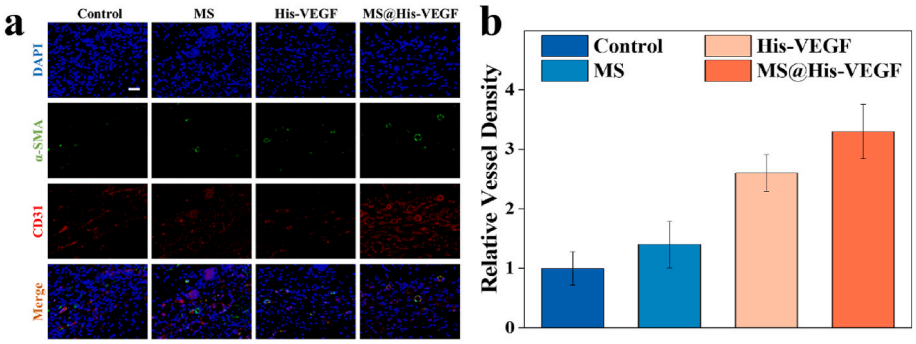

Fig. 8. Neovascularization of the tissues surrounding the wound. (a) Immunohistochemistry for CD31 and α-SMA. (b) Quantitative analysis of vessel density. The scale bar is 50 μm.

morphology as well as the elemental composition of the microspheres was determined by scanning electron microscopy.

4.3. Microsphere degradation experiments

The 10 mg lyophilized MS and 10 mg lyophilized MS (without UV photo-crosslinking) were weighed and then were placed separately into 2 ml PBS at 37 °C. At the designed time, after removing the PBS, the remaining microcapsules were freeze-dried and then their weight was measured. The degradation of MS was determined by the ratio of the residual weight to the initial weight.

4.4. In vitro drug release capacity

Equal amounts of MS and MS (without UV photo-crosslinking) were placed in PBS solutions containing the same concentrations of VEGF and His-VEGF, respectively. The supernatant was taken and the VEGF content in the supernatant was measured according to the instructions of the VEGF ELISA kits, and the loading efficiency of MS was calculated from the loss of VEGF in the supernatant. Afterwards, the supernatant was discarded and an equal volume of PBS was added and incubated at 4 °C. VEGF concentrations in the leachate were measured at 6, 12, and 24 h, and at fixed times for the following 7 d. We evaluated the effect of both

double cross-linked MS and single cross-linked MS on the release rate of VEGF and His-VEGF. The release curves were plotted by Origin.

To investigate the release profiles of Zn^{2+} from MS, the samples were submerged in a 1 ml PBS solution and kept at 37 °C for 0.5, 1, 3, 5 and 7 d. We measured the rate of Zn^{2+} release from the supernatant using ICP-AES.

4.5. Antibacterial test

E. coli and *S. aureus* were sourced from our laboratory and cultured using Luria-Bertani (LB) medium. The MS, MS@His-VEGF and was co-cultured with bacterial medium for 2 h, and an equal volume of sterile PBS was added to the control group. After diluting the bacterial solution 100,000 times, 200 μl of the solution was evenly applied to LB solid medium. After incubation at 37 °C for 24 h, photographs were taken using a camera to count the number of colonies. After collecting the remaining bacteria, they were washed twice with PBS and stained using Live & Dead Bacterial Staining Kit stain (DASO/EyhD-III stain). We added 1 μl of DASO/EyhD-III stain per 100 μl of bacterial solution and incubated the resulting solution for 20 min away from light. The bacterial solution was dropped on a slide and the bacterial survival was observed using a fluorescent microscope. The treated bacteria were collected and fixed in 2.5% glutaraldehyde for 12 h. Bacteria at the end of fixation were gradient dehydrated in different concentrations of alcohol, gold sprayed on the surface and microscopic morphology was observed under SEM.

4.6. Cytocompatibility test

The prepared MS and MS@His-VEGF were placed in a serum-free DMEM medium and incubated, after which they were filtered using a 0.22 μm filter. Cells were digested using 0.25% trypsin and counted using the cell counting plate. The cells were resuspended using a serum-free DMEM medium, DMEM containing His-VEGF, MS leachate, and MS@His-VEGF leachate, respectively. The cell density was adjusted to 50,000 cells/ml and inoculated in 96-well plates at 200 μl per well with 5 replicates per group. Cell activity was evaluated using Calcein-AM/PI staining as well as the CCK8 kit. The Calcein-AM/PI stain comprised 5 μl of Calcein-AM and 12.5 μl of PI using PBS diluted to a 5 ml configuration, with 100 μl added to each well of a 96-well plate. After incubation at 37 °C for 15 min protected from light, fluorescence photographs were taken using a fluorescence microscope. CCK8 reagent 96-well plates at 10 μl per well were incubated at 37 °C for 2 h, and then the absorbance values were detected at 450 nm band using an enzyme marker.

4.7. Cell scratch migration assay

After digestion of HUVECs, counts were performed using cell counting plates. The cells were resuspended using a 10% FBS + DMEM medium, cell density was adjusted to 200,000 cells/ml, and then added into 12-well plates at 1 ml per well. After 24 h of incubation at 37 °C, the cell status was observed under the microscope to ensure that the cell density was above 90%. The cells were washed twice with PBS and a straight line was drawn on the culture plate using 10 μl tip. Cells were washed twice again with PBS and imaged using a microscope. After that, the leaching solution from the microspheres was added at 1 ml per well and three replicate wells were set up for each group. The control group was added as equal volumes of serum-free DMEM medium. The cells were cultured for 24 h and then imaged again using a microscope. The migration ability of the cells was assessed using ImageJ software.

4.8. Tube formation assay

The Matrigel matrix gel was placed for one night in advance in a 4 °C refrigerator to re-warm. All items used in this experiment needed to be pre-cooled at 4 °C in advance. The Matrigel matrix was spread on a 96-well plate at 50 μl per well, and the plate was placed in a 37 °C cell incubator for 2 h. Cells were resuspended using microsphere leachate and cell density was adjusted to 200,000 cells/ml. Cells were added into 96-well plates lined with Matrigel matrix gel at 100 μl per well. After an 6 h incubation, cells were stained using a Calcein-AM staining solution (1 μl Calcein-AM diluted to 1 ml using PBS), 100 μl per well, and incubated for 15 min protected from light. They were imaged with a fluorescent microscope. The tube-forming ability of HUVEC was assessed using ImageJ software.

4.9. Animal experiment

In this study, the wound healing-promoting properties of MS@His-VEGF were evaluated using mice infected skin defects model. Mice were anesthetized, and after dorsal debridement, an infected skin defect model was established with a wound diameter of approximately 15 mm, and 10^7 CFU of *S. aureus* was injected. PBS, His-VEGF, MS, and MS@His-VEGF were given after 6 h. The His-VEGF group was supplemented with a single dose on day 3. Each mouse was housed in a separate cage and wound healing was recorded by taking photographs at the same time every alternate day. On day 9, the mice were euthanized and skin tissues around the wounds were obtained for subsequent experiments. The tissue specimens were fixed with 4% paraformaldehyde solution and sections were stained.

4.10. Hemolysis test

The prepared MS and MS@His-VEGF were put into a PBS solution and soaked at 37 °C for 24 h to obtain the soaking solution. At the time of execution of the mice, whole blood was obtained using a blood collection tube containing heparin and centrifuged at 1500 rpm for 5 min to obtain blood cell precipitate. The blood cells were washed 2–3 times with PBS. A 10% blood cell solution using PBS was then prepared. 50 μl of blood cells were taken and added to 950 μl of distilled water as a positive control group. 500 μl of 10% blood cells were taken and 500 μl of PBS was added as a negative control. For the experimental group, 500 μl of the microsphere leaching solution was added. It was incubated at 37 °C for 2 h and then centrifuged at 2500 rpm for 5 min; subsequently, hemolysis was observed.

Credit author statement

B.F. and L.L. conceived and designed the study. Y.J. and X.Y. performed the experiments. H.Z. and M.D. analyzed the data. Y.J. prepared the manuscript. All authors have read and approved the final manuscript.

Declaration of competing interest

There are no conflicts of interest to declare.

Data availability

Data will be made available on request.

Acknowledgements

This study was supported by Medical and Health Research Project of Zhejiang Province (No.2022KY354).

Appendix A. Supplementary data

Supplementary data related to this article can be found at https://doi.org/10.1016/j.mtbio.2023.100739.

References

[1] I. Pastar, N.C. Balukoff, J. Marjanovic, V.Y. Chen, R.C. Stone, M. Tomic-Canic, Molecular pathophysiology of chronic wounds: current state and future directions, C.S.H. Perspect. Biol. 15 (2023).

[2] B.H. Shan, F.G. Wu, Hydrogel-based growth factor delivery platforms: strategies and recent advances, Adv. Mater. (2023), e2210707.

[3] C.K. Sen, Human wound and its burden: updated 2020 compendium of estimates, Adv. Wound Care 10 (2021) 281–292.

[4] M. Mirhaj, S. Labbaf, M. Tavakoli, A. Seifalian, An overview on the recent advances in the treatment of infected wounds: antibacterial wound dressings, Macromol. Biosci. 22 (2022), e2200014.

[5] P. Kaiser, J. Wachter, M. Windbergs, Therapy of infected wounds: overcoming clinical challenges by advanced drug delivery systems, Drug. Deliv. Transl. Res. 11 (2021) 1545–1567.

[6] R. Yu, H. Zhang, B. Guo, Conductive biomaterials as bioactive wound dressing for wound healing and skin tissue engineering, Nano-Micro Lett. 14 (2021) 1.

[7] Y. Liang, Y. Liang, H. Zhang, B. Guo, Antibacterial biomaterials for skin wound dressing, Asian J. Pharm. Sci. 17 (2022) 353–384.

[8] M.D. Caldwell, Bacteria and antibiotics in wound healing, Surg. Clin. North. Am. 100 (2020) 757–776.

[9] Y. Liang, J. He, B. Guo, Functional hydrogels as wound dressing to enhance wound healing, ACS Nano 15 (2021) 12687–12722.

[10] Y. Ju, Y. Hu, P. Yang, X. Xie, B. Fang, Extracellular vesicle-loaded hydrogels for tissue repair and regeneration, mater, Today Bio 18 (2023), 100522.

[11] M. Su, L. Ruan, X. Dong, S. Tian, W. Lang, M. Wu, Y. Chen, Q. Lv, L. Lei, Current state of knowledge on intelligent-response biological and other macromolecular hydrogels in biomedical engineering: a review, Int. J. Biol. Macromol. 227 (2023) 472–492.

[12] L. Lei, Y. Zhu, X. Qin, S. Chai, G. Liu, W. Su, Q. Lv, D. Li, Magnetic biohybrid microspheres for protein purification and chronic wound healing in diabetic mice, Chem. Eng. J. 425 (2021).

[13] L. Yang, X. Wang, Y. Yu, L. Shang, W. Xu, Y. Zhao, Bio-inspired dual-adhesive particles from microfluidic electrospray for bone regeneration, Nano Res. 16 (2023) 5292–5299.

[14] H. Wang, Y. Liu, Z. Chen, L. Sun, Y. Zhao, Anisotropic structural color particles from colloidal phase separation, Sci. Adv. 6 (2020), eaay1438.

[15] H. Wang, Z. Zhao, Y. Liu, C. Shao, F. Bian, Y. Zhao, Biomimetic enzyme cascade reaction system in microfluidic electrospray microcapsules, Sci. Adv. 4 (2018), eaat2816.

[16] Q. Qu, W. Cheng, X. Zhang, H. Ravanbakhsh, G. Tang, A. Zhou, D. Pei, R. Xiong, C. Huang, Glucose-responsive enzymatic cascade microreactors in gas-shearing microfluidics microcapsules, Adv. Mater. Technol. 8 (2022).

[17] G. Tang, R. Xiong, D. Lv, R.X. Xu, K. Braeckmans, C. Huang, S.C. De Smedt, Gas-shearing fabrication of multicompartmental microspheres: a one-step and oil-free approach, Adv. Sci. 6 (2019), 1802342.

[18] C. Yang, X. Ding, C. Yang, L. Shang, Y. Zhao, Marine polymers-alginate/chitosan composited microcapsules for wound healing, Chem. Eng. J. 456 (2023).

[19] M.F.P. Graça, S.P. Miguel, C.S.D. Cabral, I.J. Correia, Hyaluronic acid-based wound dressings: a review, Carbohyd. Polym. 241 (2020), 116364.

[20] C.C.L. Schuurmans, M. Mihajlovic, C. Hiemstra, K. Ito, W.E. Hennink, T. Vermonden, Hyaluronic acid and chondroitin sulfate (meth)acrylate-based hydrogels for tissue engineering: synthesis, characteristics and pre-clinical evaluation, Biomaterials 268 (2021), 120602.

[21] B. Tao, C. Lin, X. Qin, Y. Yu, A. Guo, K. Li, H. Tian, W. Yi, D. Lei, Y. Chen, L. Chen, Fabrication of gelatin-based and Zn(2+)-incorporated composite hydrogel for accelerated infected wound healing, mater, Today Bio 13 (2022), 100216.

[22] W. Wang, M. Liu, M. Shafiq, H. Li, R. Hashim, M. El-Newehy, H. El-Hamshary, Y. Morsi, X. Mo, Synthesis of oxidized sodium alginate and its electrospun bio-hybrids with zinc oxide nanoparticles to promote wound healing, Int. J. Biol. Macromol. 232 (2023), 123480.

[23] T.R. Johnson, B.I. Gomez, M.K. McIntyre, M.A. Dubick, R.J. Christy, S. E. Nicholson, D.M. Burmeister, The cutaneous microbiome and wounds: new molecular targets to promote wound healing, Int. J. Mol. Sci. 19 (2018).

[24] P. Pino, F. Bosco, C. Mollea, B. Onida, Antimicrobial nano-zinc oxide biocomposites for wound healing applications: a review, Pharmaceutics 15 (2023).

[25] L. Sukhodub, M. Kumeda, L. Sukhodub, V. Bielai, M. Lyndin, Metal ions doping effect on the physicochemical, antimicrobial, and wound healing profiles of alginate-based composite, Carbohyd. Polym. 304 (2023), 120486.

[26] F. Yang, Y. Xue, F. Wang, D. Guo, Y. He, X. Zhao, F. Yan, Y. Xu, D. Xia, Y. Liu, Sustained release of magnesium and zinc ions synergistically accelerates wound healing, Bioact. Mater. 26 (2023) 88–101.

[27] R.S. Apte, D.S. Chen, N. Ferrara, VEGF in signaling and disease: beyond discovery and development, Cell 176 (2019) 1248–1264.

[28] M. Zubair, J. Ahmad, Role of growth factors and cytokines in diabetic foot ulcer healing: a detailed review, Rev. Endocr. Metab. Disord. 20 (2019) 207–217.

[29] M. Hajialyani, D. Tewari, E. Sobarzo-Sánchez, S.M. Nabavi, M.H. Farzaei, M. Abdollahi, Natural product-based nanomedicines for wound healing purposes: therapeutic targets and drug delivery systems, Int. J. Nanomed. 13 (2018) 5023–5043.

[30] Z. Xiong, L. Sun, H. Yang, Z. Xiao, Z. Deng, Q. Li, C. Wang, F. Shen, Z. Liu, Ni-Alginate hydrogel microspheres with sustained interleukin 2 release to boost cytokine-based cancer immunotherapy, Adv. Funct. Mater. 33 (2022).

[31] H. Henriques-Antunes, R.M.S. Cardoso, A. Zonari, J. Correia, E.C. Leal, A. Jimenez-Balsa, M.M. Lino, A. Barradas, I. Kostic, C. Gomes, J.M. Karp, E. Carvalho, L. Ferreira, The kinetics of small extracellular vesicle delivery impacts skin tissue regeneration, ACS Nano 13 (2019) 8694–8707.

[32] T. Tanaka, M. Narazaki, T. Kishimoto, IL-6 in inflammation, immunity, and disease, C.S.H. Perspect. Biol. 6 (2014) a016295.

[33] E.A. Burian, L. Sabah, T. Karlsmark, K. Kirketerp-Møller, C.J. Moffatt, J.P. Thyssen, M.S. Ågren, Cytokines and venous leg ulcer healing-A systematic review, Int. J. Mol. Sci. 23 (2022).

[34] G. Broughton 2nd, J.E. Janis, C.E. Attinger, Wound healing: an overview, Plast. Reconstr. Surg. 117 (2006) 1e. S-32e-S.